

# Observations of the CO dayglow at 4.7 $\mu\text{m}$ on Mars: Variations of temperature and CO mixing ratio at 50 km



Vladimir A. Krasnopolsky <sup>\*,1</sup>

Department of Physics, Catholic University of America, Washington, DC 20064, USA  
Moscow Institute of Physics and Technology, Dolgoprudnyy 141700, Russia

## ARTICLE INFO

### Article history:

Received 27 July 2013

Revised 5 October 2013

Accepted 8 October 2013

Available online 18 October 2013

### Keywords:

Mars, atmosphere

Mars, climate

Atmospheres, composition

Spectroscopy

## ABSTRACT

The CO (2-1) and (1-0) dayglow at 4.7  $\mu\text{m}$  was observed on Mars at the peak of northern summer ( $L_S = 110^\circ$ ) using the CSHELL spectrograph at NASA IRTF. There are six (2-1) and two (1-0) emission lines in the observed spectra. They are contaminated by the solar CO lines and some martian and telluric lines. Fitting by synthetic spectra results in intensities of the dayglow lines and reflectivities of Mars at 4.7  $\mu\text{m}$ . Mean reflectivity at 109°W from 50°S to 50°N is 0.15, similar to that observed by Mariner 6 and 7 in four regions on Mars. The CO (1-0) dayglow is excited by absorption of sunlight at 4.7  $\mu\text{m}$ ; the emission is optically thick with a non-LTE line distribution and peaks near 87 km. The (1-0) line intensities are converted to the (1-0) band intensity using the line distribution from Billebaud et al. (1991). Mean intensity of the CO (1-0) dayglow is 1.7 MR with a weak limb darkening to 1.3 MR. This dayglow is poorly accessible for diagnostics of the martian atmosphere. The CO (2-1) dayglow is excited by absorption of the sunlight by the CO (2-0) band at 2.35  $\mu\text{m}$  with minor contributions from photolysis of CO<sub>2</sub> and the CO (3-0) band at 1.58  $\mu\text{m}$ . The dayglow is quenched by CO<sub>2</sub> and peaks at 50 km. Intensities of the observed six (2-1) lines result in rotational temperatures that should be equal to ambient temperatures at 50 km. These temperatures are retrieved from 50°S to 90°N and vary in the range of 140–170 K with a mean value of 153 K. The observed intensities of the CO (2-1) dayglow are corrected for airmass and the surface reflection and give vertical intensities that are equal to 2.1 MR at 20°N to 50°N decreasing to 1.5 MR at 90°N and 1 MR at 45°S. The dayglow intensities depend on CO mixing ratio at 50 km and solar zenith angle. Retrieved CO mixing ratios at 50 km gradually increase from 1100 ppm at 40°S to 1600 ppm at 70°N. This behavior is very different from that observed in the lowest scale height at the same season with increase to southern polar regions because of condensation of CO<sub>2</sub> near the south pole (Krasnopolsky, V.A. [2003]. *Icarus* 165, 315–325). The difference reflects complicated dynamic processes in the atmosphere. This is the first observation of CO in the middle atmosphere of Mars, and the observed behavior of CO should be further studied in both observation and theory. The CO (2-1) dayglow is a tool for remote sensing of temperature and CO at 50 km on Mars using ground-based and spacecraft instruments. The observed CO and temperatures may be used to test photochemical GCMs for Mars.

© 2013 Elsevier Inc. All rights reserved.

## 1. Introduction

The CO (2-1) and (1-0) dayglow at 4.7  $\mu\text{m}$  was detected on Mars by Billebaud et al. (1991) using the high-resolution Fourier Transform Spectrometer at the Canada–France–Hawaii Telescope. The measured dayglow intensities were uncertain within a factor of 3 ( $2.4^{+2}_{-1}$  MR and  $1.3^{+1.1}_{-0.6}$  MR, respectively) and referred to the whole martian disk. The authors identified mechanisms of the dayglow

excitation: absorption of the solar light by the CO (1-0), (2-0) and (3-0) bands at 4.7, 2.35 and 1.58  $\mu\text{m}$ , respectively, and photolysis of CO<sub>2</sub>. Currently spectra of the CO dayglow are measured by the Planetary Fourier Spectrometer (Formisano et al., 2006) at the Mars Express orbiter, and some MEX observations of the martian CO dayglow were compared with those on the Earth and Venus by Gilli et al. (2011). However, the PFS spectral resolution is insufficient for the nadir observations of the CO dayglow, while the limb observations are restricted by the instrument field of view of 60 km at the best orbits.

Here we will discuss our ground-based spatially-resolved observations of the CO dayglow on Mars, our reanalysis of the excitation processes, and retrieval of temperatures and CO mixing ratios at 50 km from the observed data. The derived CO mixing ratios will be compared with those in the lowest scale height on Mars.

\* Address: 6100 Westchester Park Drive #911, College Park, MD 20740, USA. Fax: +1 202 319 4448.

E-mail address: [vlad.krasn@verizon.net](mailto:vlad.krasn@verizon.net)

<sup>1</sup> Visiting Astronomer at the Infrared Telescope Facility, which is operated by the University of Hawaii under Cooperative Agreement No. NCC 5-538 with the National Aeronautic and Space Administration, Science Mission Directorate, Planetary Astronomy Program.

## 2. Observations

We observed the CO dayglow at 4.7  $\mu\text{m}$  using the long-slit cryogenic echelle spectrograph CSHELL at the NASA Infrared Telescope Facility on Hawaii, Mauna Kea. The telescope diameter is 3 m, and its location on the summit with elevation of 4.2 km, atmospheric pressure of 0.6 bar, and mean overhead water of 2 precipitable mm is favorable for spectroscopy of the planetary atmospheres.

CSHELL (Greene et al., 1993) covers a narrow spectral interval of  $0.0023\nu_0$  where the central wavenumber  $\nu_0$  may be chosen in a wide range from 1800 to 9000  $\text{cm}^{-1}$  (5.6–1.1  $\mu\text{m}$ , respectively). The instrument resolving power is  $\nu/\delta\nu = 4 \times 10^4$ . The detector is an InSb array of  $256 \times 150$  pixels cooled to 30 K. Each pixel is equal to  $9 \times 10^{-6} \nu_0$  and 0.2 arcsec in the spectral and aspect directions, respectively. Each exposure gives a frame of 150 spectra along a slit of 30 arcsec with 256 pixels in each spectrum. An effective spatial resolution of the telescope and spectrograph combination is  $\sim 1$  arcsec.

Our observations of the CO dayglow on Mars were made on May 11, 2012, when the angular diameter of Mars was 9.2 arcsec and its geocentric velocity was 13.8  $\text{km s}^{-1}$ . The spectra were acquired at three central wavenumbers  $\nu_0 = 2137, 2144, \text{ and } 2151 \text{ cm}^{-1}$ . The spectral frames cover six lines of the CO (2-1) dayglow: R4 2135.313  $\text{cm}^{-1}$ , R5 2138.911  $\text{cm}^{-1}$ , R6 2142.473  $\text{cm}^{-1}$ , R7 2145.999  $\text{cm}^{-1}$ , R8 2149.489  $\text{cm}^{-1}$ , and R9 2152.942  $\text{cm}^{-1}$ . Geocentric velocity of Mars determines the Doppler shift that was to the red by 0.099  $\text{cm}^{-1}$ . Areocentric solar longitude that determines martian season was  $L_S = 110^\circ$ , that is, near the peak of the northern summer (July 12 in the terrestrial calendar).

To get a maximal latitudinal coverage and at the same local time, we put the spectrograph slit along the central meridian on the martian disk (Fig. 1). We observed spectra of Mars, dark current, flat field from a continuum source, sky foreground 30 arcsec off Mars, and a calibration star. Thermal radiation is significant at 4.7  $\mu\text{m}$ , and the sky foreground is very bright. Typically we use stars of fourth magnitude from the IRTF catalog of bright infrared standard stars for absolute calibration. However, those stars were too weak and not seen against the bright sky foreground, and we observed Arcturus with magnitude of  $-3$  at 4.7  $\mu\text{m}$ .

## 3. Data processing and analysis

Our standard data processing involves differences between the Mars spectra and those of the foreground that are divided by differences of the flat field and dark current spectra. The obtained

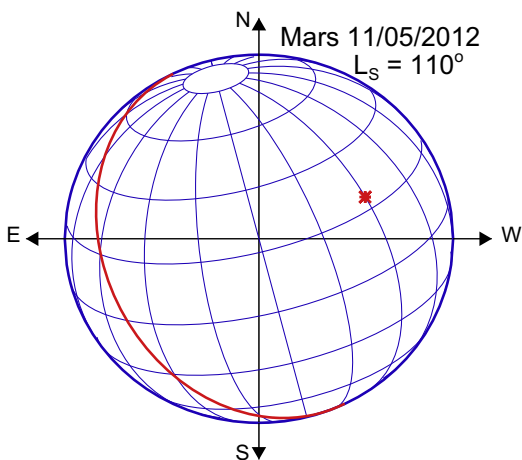


Fig. 1. Mars in the celestial coordinates as seen in our observations on May 11, 2012. Subsolar point and terminator are shown. The spectrograph slit was placed along the central meridian with a mean position at  $108^\circ\text{W}$  during the observations.

spectra are therefore corrected for the foreground and flat field. Next we search for bad pixels and replace them by mean values of their two neighbors.

We will see below that the CO dayglow lines are contaminated by the solar CO absorption lines, martian  $\text{CO}_2$  lines, and some telluric lines. Therefore fitting of the observed spectra by synthetic spectra should be made for careful extraction of the dayglow line intensities. Our technique of the fitting requires conversion of the observed spectra to a wavenumber scale with a step of  $0.001 \text{ cm}^{-1}$ . We developed a parabolic fitting of three adjacent pixels that extends a pixel to eight sampling points and keeps the sum of these points at the pixel reading (Krasnopolsky, 2007; Krasnopolsky et al., 2013). The standard parabolic fitting fixes the middle sampling point at the pixel reading. Then wavenumber scales are determined using identified lines, and the spectra are linearly interpolated to the step of  $0.001 \text{ cm}^{-1}$ .

The processed and calibrated spectra observed at the equator are shown in Fig. 2. The spectral continuum is thermal emission of the martian surface and reflected solar light. The CO (2-1) dayglow lines are well seen in the spectra. They become very prominent at high latitudes where the continuum is weak. Martian CO and  $\text{CO}_2$  absorption lines are Doppler-shifted to the red by 0.099  $\text{cm}^{-1}$ . They are identified in the spectra along with telluric lines of  $\text{H}_2\text{O}$  and  $\text{N}_2\text{O}$ . Weak telluric ozone lines are present as well.

Column abundances of  $\text{CO}_2$  and CO on Mars exceed those on the Earth by two orders of magnitude. Therefore telluric lines of these species are weak in the spectra. Exceptions are the strong CO (1-0) P2, P1, and R1 lines at 2135.546, 2139.426, and 2150.856  $\text{cm}^{-1}$ , respectively (Fig. 2). The P1 line is contaminated by a strong telluric  $\text{H}_2\text{O}$  line; P2 and R1 are shown in Fig. 3. The lines demonstrate complicated structures with three absorption peaks. The line strengths are  $2.7 \times 10^{-19} \text{ cm}$ , the martian lines are thermally broadened, its full width at half maximum (FWHM) is  $0.004 \text{ cm}^{-1}$ , and the optical depth is  $\sim 10^4$  at the line center. Intensity at the line center should reflect thermal radiation at a level of  $\tau \approx 1$ . This level is near 85 km with  $T \approx 130 \text{ K}$ , and the intensity is very low. The telluric line is collisionally broadened with  $\text{FWHM} \approx 0.06 \text{ cm}^{-1}$ , optical depth is  $\approx 5$  at the line center, and the line is observed in pure absorption because of the foreground correction (Krasnopolsky, 2007). The observed structure is perfectly explained by dayglow emissions at the martian line centers (Fig. 3).

Thus our observations cover six emission lines of the CO (2-1) dayglow and two lines of the CO (1-0) dayglow. The CO (2-1) band is hot and may only be absorbed by aerosol in the martian atmosphere. Evidently the surface reflection increases the observed emissions of the CO (2-1) dayglow. However, CO absorption lines are strong in the solar spectrum, while their Doppler shift relative to the dayglow lines is due to Mars heliocentric velocity and therefore low. These solar absorption lines are opposite to the observed (2-1) dayglow emission lines and significantly reduce their apparent intensities.

Radiation of Mars at 4.7  $\mu\text{m}$  is a sum of thermal emission and the reflected sunlight, and it is not easy to separate the components. We have found in the literature reflectivities of four regions on Mars (Erard and Calvin, 1997) that are based on the Mariner 6 and 7 observations in 1969. Those data are insufficient for our analysis, and we will try to get Mars' reflectivities as parameters in the spectral fitting.

High-resolution solar infrared spectra were observed by the ATMOS (Farmer and Norton, 1989) and ACE (Hase et al., 2010) orbiters with resolution 0.01 and 0.02  $\text{cm}^{-1}$ , respectively. The ACE spectrum near the CO (2-1) R6 line and a version of the ATMOS spectrum suggested by Kurucz (2011, <http://kurucz.harvard.edu/sun/atmos/>) are shown in Fig. 4. Evidently the solar absorption lines are deeper and narrower in the ATMOS spectrum because

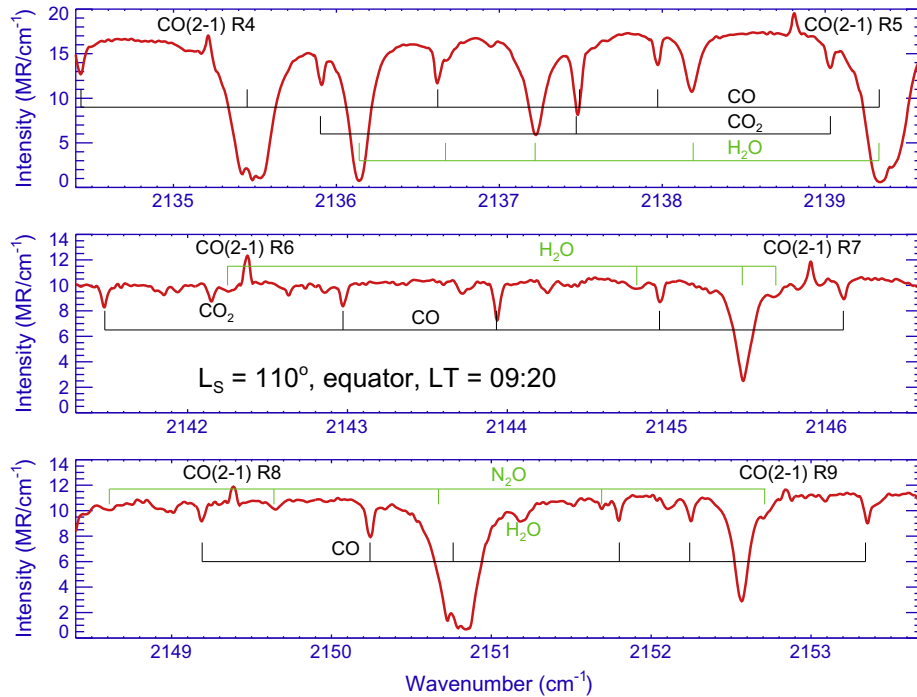


**Fig. 2.** Observed spectra of Mars at the equator. The CO (2-1) dayglow lines are seen. The martian lines of CO and CO<sub>2</sub> are Doppler-shifted to the red by  $0.099 \text{ cm}^{-1}$ . Telluric lines of H<sub>2</sub>O and N<sub>2</sub>O are identified.

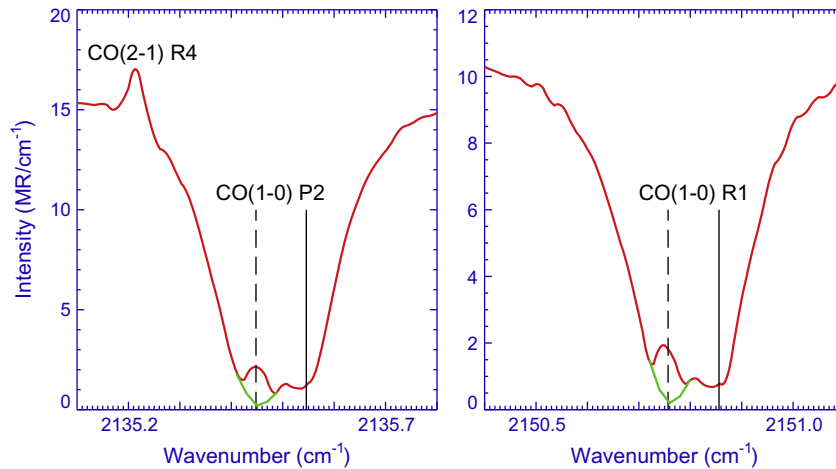


**Fig. 3.** Structure of the observed CO (1-0) P2 and R1 lines. Each line includes the telluric and martian absorptions, and the latter is Doppler shifted to the red. The dayglow emissions are seen at the centers of the martian lines. Green curves show the expected shapes of the martian absorption lines without the dayglow emissions. The rest and Doppler-shifted positions of the CO lines are shown by the vertical lines. (For interpretation of the references to color in this figure legend, the reader is referred to the web version of this article.)

of the better spectral resolution. The ATMOS spectrum perfectly fits the CO (2-1) R6 line position from HITRAN 2012 (Rothman et al., 2013) while the ACE spectrum is shifted to the red by  $0.007 \text{ cm}^{-1}$ . Although it is possible to apply this correction and use the ACE spectrum, we choose the ATMOS spectrum for our spectral fits. The uncorrected ACE spectrum results in a significant degradation of our spectral fitting.

Adjustments to the observed spectra involve parabolic corrections to the continuum (3 parameters), a sinusoidal term (3 parameters: amplitude, period, and phase), and scattered light. Three wavenumber corrections are applied to the center and edges of a spectrum, that is, 10 parameters total. Synthetic spectra are calculated using abundances of CO and CO<sub>2</sub> on Mars and their mean

temperature (3 parameters), telluric H<sub>2</sub>O and its mean temperature and pressure (3 parameters), telluric CO, solar-to-thermal emission ratio in a spectrum, 3 dayglow line intensities (2 dayglow intensities for the spectrum in the middle panel of Fig. 2), and the instrument spectral resolution, that is, 12 parameters total. The overall 22 parameters are much smaller than 256 degrees of freedom (pixels) in each spectrum.

The synthetic spectra also involve weak (less than 1%) absorptions by telluric CO<sub>2</sub> and O<sub>3</sub> that are calculated using their fixed mean abundances, temperatures, and pressures. Absorptions by the martian CO and CO<sub>2</sub> are calculated using the Voigt line shape with half surface pressure that is taken from the MGS/TES observations (Smith, 2004). The achieved accuracy of the fitting is  $\sim 1\%$ .

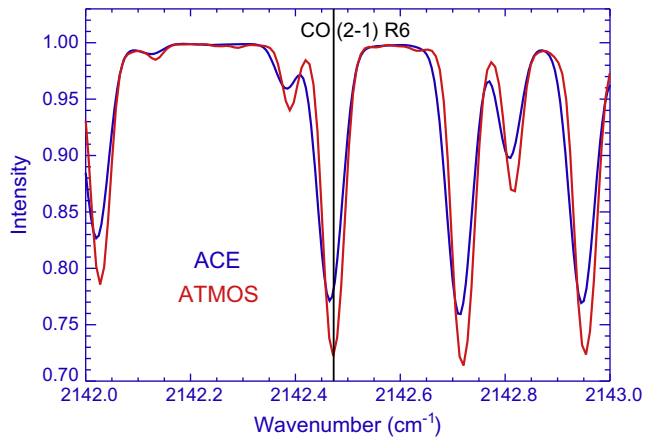


**Fig. 4.** High-resolution solar spectra near the CO (2-1) R6 line observed using ACE (Hase et al., 2010) and ATMOS (Kurucz, 2011). The ACE spectrum is shifted to the red by  $0.007 \text{ cm}^{-1}$  from the HITRAN 2012 line position. Depths of the solar absorption lines are different in the spectra because of the different spectral resolution of the instruments. (For interpretation of the references to color in this figure legend, the reader is referred to the web version of this article.)

#### 4. Results

The retrieved reflectivity of Mars along the central meridian at  $109^\circ\text{W}$  is shown in Fig. 5. The values are obtained using our absolute calibration, the solar radiation of  $0.50 \text{ mW cm}^{-2} \mu\text{m}^{-1}$  at  $4.68 \mu\text{m}$  at 1 AU from Pierce and Allen (1977), and assuming the Lambert reflection. The measured reflectivities include effects of water ice clouds that are significant in this season ( $L_s = 110^\circ$ ) with a typical optical depth of 0.1 at  $12 \mu\text{m}$  (MGS/TES data, Smith (2004)). Then expected contribution from the water ice clouds to the observed reflectivities is of the order of 0.01, taking into account forward scattering of the particles. The observed reflectivities may be compared with those in four regions from Erard and Calvin (1997): 0.12, 0.15, 0.17, and 0.19. The regions are at low latitudes and do not overlap our observations. Their mean value of 0.16 is similar to those in our observations at low and middle latitudes.

Airglow line intensity  $I$  is proportional to population of the upper rotational state, its statistical weight  $2J + 1$  ( $J$  is the rotational quantum number), and transition probability  $A$ . Below we confirm the conclusion from Billebaud et al. (1991) that the rotational population in the CO (2-1) dayglow is in local thermodynamic equilibrium, conforms to the Boltzmann law, and is proportional to  $e^{-\frac{E}{kT}} = e^{-\frac{B}{kT}}$ . Here  $E = B J(J + 1)$  is the rotational energy,  $B = 1.89 \text{ cm}^{-1}$  is the rotational constant for CO ( $\nu = 2$ ), and  $\alpha = 1.4388 \text{ cm K}$ . Fig. 6 shows log of rotational population versus rotational energy. This plot is a straight line, and its slope determines rotational temperature  $T = 151 \pm 6 \text{ K}$ . We will discuss below that rotational temperature of the CO (2-1) dayglow corresponds to the ambient temperature at 50 km.

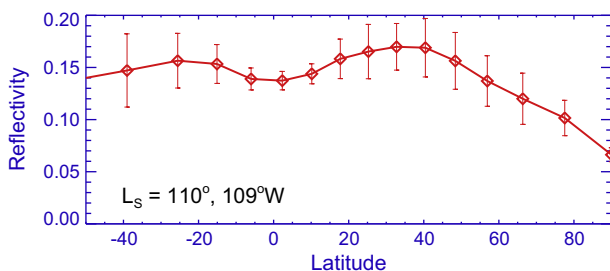


**Fig. 5.** Observed reflectivity of Mars at  $4.7 \mu\text{m}$  along  $109^\circ\text{W}$ .

Retrieved latitudinal distribution of atmospheric temperature at 50 km is shown in Fig. 7. The temperature varies from 140 to 170 K with a mean value of 153 K. The observations refer to the northern summer, and temperatures in the northern hemisphere at  $0\text{--}50^\circ$  are higher than those in the southern hemisphere at the similar latitudes.

The measured temperatures at 50 km may be compared with those retrieved from MGS/TES (Smith, 2004) and MRO/MCS (McCleese et al., 2010) limb observations. The MGS/TES temperatures at 50 km observed in March 1999 at  $L_s = 110\text{--}115^\circ$  between longitudes  $60\text{--}160^\circ\text{W}$  (centered at our longitude of  $109^\circ\text{W}$ ) have been averaged and shown in Fig. 7. These observations were not so detailed at  $L_s \approx 110^\circ$  in 2001 and 2003, and we do not show them. Reproduction of the MRO/MCS temperatures at 50 km requires a conversion of their color code to numerical values. Their mean temperatures are  $140\text{--}150 \text{ K}$ , close to our mean temperature of 153 K.

Results of the LMD general circulation model (Forget et al., 1999) are available as the Mars Climate Database ([http://www-mars.lmd.jussieu.fr/mcd\\_python/](http://www-mars.lmd.jussieu.fr/mcd_python/)) and shown in Fig. 7 for the conditions of our observations. The maximal difference between our temperatures and those from TES and MCD is 27 K at  $40^\circ\text{N}$ ; here the TES and MCD data overlap. The maximal difference between the MCD temperatures and those from TES and ours is 16 K at  $40^\circ\text{S}$ ; here our and TES data coincide. Overall, there is a reasonable agreement between the retrieved temperatures at 50 km and the existing data.

According to our calculations, a sum of six CO (2-1) dayglow lines R4 to R9 is equal to a quarter of the total dayglow intensity at  $120\text{--}200 \text{ K}$ . Latitudinal variations of the observed total CO (2-1) intensity are shown in Fig. 8. The observed intensity  $4\pi I_o$  should be corrected for observing angle  $\varphi$  and the surface reflection  $a$  to get a true vertical intensity  $4\pi I$  (Krasnopolsky, 2003):

$$4\pi I = \frac{4\pi I_o}{(1/\cos \varphi)_c + 2a}$$

Here  $(1/\cos \varphi)_c$  means that this function is convolved by the instrument spatial resolution that is approximated by a Gaussian with a FWHM of 1 arcsec. The corrected vertical intensity of the CO (2-1) dayglow is  $\sim 2 \text{ MR}$  from the equator to  $65^\circ\text{N}$  and diminishes to the higher latitudes. The mean intensity is  $1.85 \text{ MR}$ , close to  $2.4_{-1}^{+2} \text{ MR}$  in Billebaud et al. (1991).

According to the radiative transfer calculations by Billebaud et al. (1991), the CO (1-0) dayglow peaks at 87 km and its rotational distribution is broader than that expected for  $T \approx 130 \text{ K}$  typical of these altitudes because of the non-LTE effects. However,

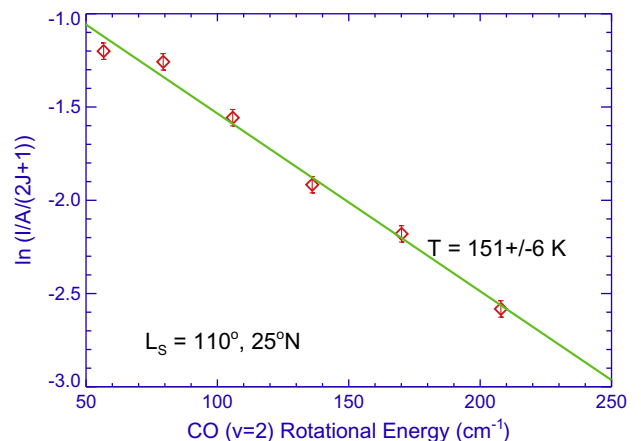


**Fig. 6.** Retrieval of rotational temperature of the CO (2-1) dayglow at  $4.7 \mu\text{m}$  using the observed six emission lines.

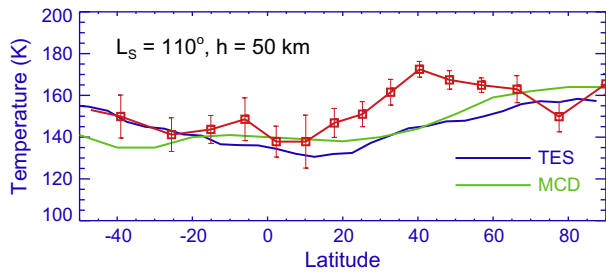


**Fig. 7.** Observed latitudinal distribution of temperature at 50 km is compared with those from the MGS/TES limb observations (Smith, 2004) and computed by the Mars Climate Database.

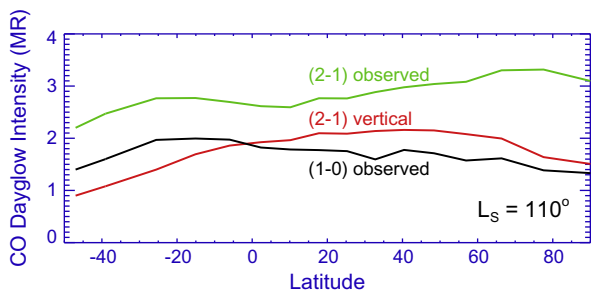


**Fig. 8.** Observed total intensities of the CO (2-1) and (1-0) dayglow.

sums of the P2 and R1 lines occasionally coincide and are equal to 0.077 of the total dayglow for both the rotational distribution from Billebaud et al. (1991) and that for 130 K. The observed total CO (1-0) dayglow is also shown in Fig. 8. Its mean intensity is 1.7 MR, within uncertainties of the value of  $1.3_{-0.6}^{+1.1}$  MR from Billebaud et al. (1991).

## 5. Excitation of the CO dayglow at 4.7 $\mu\text{m}$

Rate coefficient of quenching of  $\text{CO}(v=1)$  by  $\text{CO}_2$  was measured by Starr and Hancock (1975) at a few temperatures between 163 and 406 K. Their results may be presented as  $k = 5.3 \times 10^{-13} - e^{-525/T} \text{ cm}^3 \text{ s}^{-1}$ . The  $\text{CO}_2$  densities are  $\sim 10^{13} \text{ cm}^{-3}$  near the peak of the CO (1-0) dayglow at 87 km, and the quenching rate  $k [\text{CO}_2] \approx 0.1 \text{ s}^{-1}$  is much smaller than the CO (1-0) transition probability of  $\sim 20 \text{ s}^{-1}$ . Brightness of a conservatively scattering optically thick medium weakly depends on its optical depth; therefore the CO (1-0) dayglow is almost insensitive to the CO mixing ratio. Billebaud et al. (1991) calculated the CO (1-0) rotational distribution, which is non-LTE and cannot describe the local temperature. Therefore this dayglow is poorly accessible for diagnostics of the martian atmosphere. More promising is the CO (2-1) dayglow, which will be discussed here in more detail. Billebaud et al. (1991) considered excitation of  $\text{CO}(v=2)$  by photolysis of  $\text{CO}_2$  and absorption of the solar light by the CO (2-0) and (3-0) bands at 2.35 and 1.57  $\mu\text{m}$ , respectively. Here we will update and make some improvements to their analysis.

### 5.1. Vertical profiles of the CO mixing ratio

We need CO vertical profiles with various mixing ratios in the lowest scale height for modeling of the CO dayglow and its column intensity, and these profiles are lacking. While the chemical balance of CO on Mars looks simple with production by photolysis of  $\text{CO}_2$  and loss in the reaction with OH, the photochemical models predict abundances of CO in the martian lower atmosphere that are smaller by a factor of 8 than the observed values (see Krasnopolsky (2010) and references therein). Photochemical GCMs cannot

run for  $\sim 1000$  years to reproduce properly abundances of the long-living photochemical products ( $\text{O}_2$ , CO, and  $\text{H}_2$ ), and total amounts of these species are adopted in those GCMs. Therefore the problem of CO remains unsolved in the martian atmosphere.

Both Viking observations (Nier and McElroy, 1977) and photochemical models give the CO mixing ratio of  $\sim 1\%$  near the ionospheric peak at  $\sim 130$  km. We calculate these profiles assuming mean dayside (that is, for the solar zenith angle of  $60^\circ$ ) production of CO by photolysis of  $\text{CO}_2$  and varying the CO mixing ratio near the surface. The calculated profiles are shown in Fig. 9. Eddy diffusion and other details of the calculations may be found in Krasnopolsky (2010).

### 5.2. Excitation of the CO dayglow by photolysis of $\text{CO}_2$

We have not found laboratory studies of vibrational excitation of CO by photolysis of  $\text{CO}_2$  in the literature. Billebaud et al. (1991) argued that energy of the  $\text{CO}(v=2)$  excitation is much smaller than a typical photon excess energy in photolysis of  $\text{CO}_2$ . Therefore almost all photolysis events result in excitations of  $\text{CO}(v \geq 2)$ . The  $\Delta v = 1$  transitions are much stronger than those for  $\Delta v \geq 2$  (by a factor of  $\approx 60$  in CO), and all  $\text{CO}(v \geq 2)$  either are quenched or emit the (2-1) dayglow by cascading. Then the  $\text{CO}_2$  dayside mean photolysis column rate of  $1.5 \times 10^{12} \text{ cm}^{-2} \text{ s}^{-1}$  on Mars (Krasnopolsky, 2010) corresponds to the CO (2-1) dayglow excitation rate of 1.5 MR.

Considering the problem in more detail, we adopt that the photon excess energy corrected for the electronic excitation of O and CO is equally distributed over all degrees of freedom. This is a natural and standard assumption in the lack of the data. The momentum conservation requires equal momentums of CO and O after the photolysis. Therefore the system has three translational, one rotational, and one vibrational degrees of freedom. The  $\text{CO}(v=2)$  energy is 0.53 eV, and the required excess energy to excite  $\text{CO}(v=2)$  is 2.65 eV. This adds to the  $\text{CO}_2$  dissociation energy of 5.43 eV giving a limiting photon wavelength of 153 nm. However, the  $\text{CO}_2$  dissociation to CO and O in the ground states is spin-forbidden, and the products are  $\text{CO} + \text{O}(^1\text{D})$  for  $\lambda < 168$  nm. The  $\text{O}(^1\text{D})$  energy is 1.96 eV, and this moves the limiting wavelength to 123 nm. Actually the only solar emission that excites  $\text{CO}(v \geq 2)$  in photolysis of  $\text{CO}_2$  is Lyman-alpha 121.6 nm.  $\text{O}(^1\text{S})$  is excited by Lyman-alpha with a yield of 0.1 (Slanger and Black, 1971), and the expected yield of  $\text{CO}(v=2)$  is 0.9. The yield of  $\text{O}(^1\text{S})$  increases to  $\approx 1$  at 110–114 nm, and the dissociation to  $\text{CO}(a^3\Pi)$  dominates below 108 nm.

The solar Lyman-alpha emission is  $3.7 \times 10^{11} \text{ ph cm}^{-2} \text{ s}^{-1}$  at 1 AU and mean solar activity. The  $\text{CO}_2$  cross section is

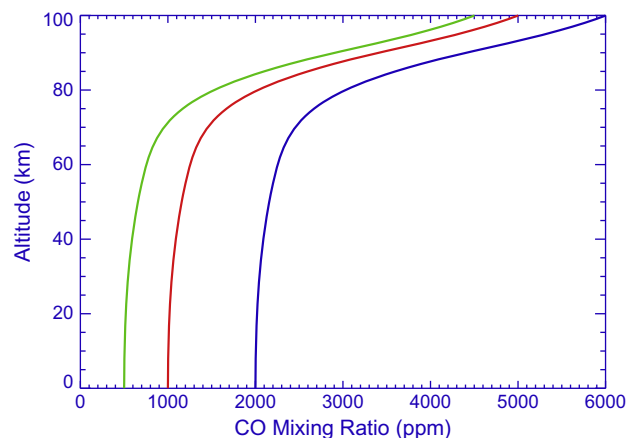


**Fig. 9.** Vertical profiles of the CO mixing ratio calculated for analysis of excitation of the CO (2-1) dayglow.

$\sigma = 4.5 \times 10^{-20} \text{ cm}^2$  at 195 K (Yoshino et al., 1996). The absorption peaks at  $N = \frac{\cos z}{\sigma} \approx 10^{19} \text{ cm}^{-2}$ , that is, near 80 km (Fig. 10) where the quenching by  $\text{CO}_2$  is negligible. The excited CO (2-1) dayglow is  $\frac{0.9 \times 370 \cos z}{R^2}$  kR, and the dayside mean intensity is 72 kR at the mean heliocentric distance  $R = 1.52 \text{ AU}$  and mean solar activity. It is smaller by an order of magnitude than that calculated by Billebaud et al. (1991) for all  $\text{CO}_2$  photolysis events.

### 5.3. Absorption of sunlight by the CO (2-0) and (3-0) bands

Absorption of the sunlight by the CO (2-0) and (3-0) bands at 2.35 and 1.58  $\mu\text{m}$  pumps the  $\nu = 2$  and 3 levels of CO, respectively, and the latter cascades to  $\nu = 2$ . This mechanism was suggested and calculated by Billebaud et al. (1991). Our calculations covered altitudes up to 100 km and applied the Voigt line shape. Temperatures and pressures were taken from Krasnopolsky (2010), CO line parameters from HITRAN 2012 (Rothman et al., 2013), pressure-broadened halfwidths for the CO lines in  $\text{CO}_2$  from Sung and Varanasi (2005), and the solar irradiances from Pierce and Allen (1977). The code involved 46 lines of CO, and each line was calculated at 40 wavenumber intervals with a step of  $0.001 \text{ cm}^{-1}$ . This step is about a quarter of the Doppler line width. The calculations were made with an altitude step of 1 km.

Quenching of  $\text{CO}(\nu = 2)$  by  $\text{CO}_2$  is generally unknown, and the closest analog is



studied by Starr and Hancock (1975). This exchange of the vibrational quantum proceeds with a rate coefficient of  $5.3 \times 10^{-13} e^{-525/T} \text{ cm}^3 \text{ s}^{-1}$  (see above). Exchange of two quanta and just vibrational quenching are not ruled out for  $\text{CO}(\nu = 2)$ , and we increase this rate coefficient by a factor of 1.5 to account for these possibilities.

Calculated vertical profiles of the CO (2-1) dayglow excited by the CO (2-0) and (3-0) bands are shown in Fig. 10. The calculations were made for the mean dayside conditions (solar zenith angle is  $60^\circ$ ). The different behavior of the excitation profiles for the two bands is because of a great difference in the band strengths. Conditions for the (2-0) band are optically thin above 70 km, while the flat region at 45–25 km with the further shallow increase to the surface is due to weak lines of the band. The (3-0) band remains unsaturated down to the surface. The profiles in Fig. 10 demonstrate some similarities and some significant differences with those calculated by Billebaud et al. (1991).

The vertical profile of the CO (2-1) dayglow is shown in Fig. 11 in the linear scale. It was calculated for the CO fraction of 1000 ppm in the lower atmosphere. Photolysis of  $\text{CO}_2$  and

absorption by the CO (3-0) band contribute 7% total to the dayglow, with the absorption by the CO (2-0) band being responsible for the bulk emission.

## 6. Variations of CO at 50 km

The CO (2-1) dayglow peaks at 50 km for the solar zenith angle of  $60^\circ$  (Fig. 11). The peak altitude varies from 48 km at  $0^\circ$  to 54 km at  $80^\circ$ . The rate coefficient of the collisional exchange of rotational excitation is  $\sim 10^{-10} \text{ cm}^3 \text{ s}^{-1}$ , the  $\text{CO}_2$  density at 50 km is  $\sim 10^{15} \text{ cm}^{-3}$ , and their product exceeds the CO (2-1) transition probability  $\sim 30 \text{ s}^{-1}$  by a few orders of magnitude. Therefore the CO (2-1) line distribution fits LTE, and the derived rotational temperatures (Fig. 7) is equal to the atmospheric temperatures near 50 km.

Calculated variations of the dayglow vertical intensity with the solar zenith angle and adopted CO mixing ratio in the lower atmosphere are shown in Fig. 12. These three curves may be used for retrieval of the CO mixing ratios at 50 km from the observed vertical intensities of the CO (2-1) dayglow (Fig. 8).

Cos $z$  is easy to calculate for our observing conditions as a scalar product of the solar vector (Fig. 1) and radius-vector of an observed point. Then three dayglow intensities are taken for this cos $z$  from the curves in Fig. 12 for three CO fractions in the lower atmosphere. These CO fractions give three CO mixing ratios at 50 km using the CO vertical profiles in Fig. 9. Finally, a CO mixing ratio at 50 km is obtained at the observed point using the parabolic interpolation between three values.

The retrieved CO mixing ratios at 50 km are shown in Fig. 13. The observed CO fraction at 50 km gradually increases from  $40^\circ\text{S}$  to  $60^\circ\text{N}$  by a factor of 1.5.

Variations in the atmospheric density profile do not affect the measured CO mixing ratios but slightly change the reference altitude from 50 km, typically within  $\pm 2 \text{ km}$ . We have tested that an uncertainty in the quenching rate coefficient changes proportionally the absolute values of the curve in Fig. 13 but does not change its shape. Random uncertainties may be evaluated using six line intensities for each observing point. They give six band intensities, their mean value and its uncertainty, which is  $\sim 5\%$ . Therefore the observed relative behavior of the CO mixing ratio at 50 km is rather accurate from  $20^\circ\text{S}$  to  $60^\circ\text{N}$ . The illumination and observing conditions significantly change within the instrument field of view near the limbs, and these points are more uncertain.

We have not found observational data on CO in the middle atmosphere of Mars in the literature. Fig. 13 reproduces our observations of CO in the lower atmosphere in March 1999 at the same season  $L_s = 112^\circ$  (Krasnopolsky, 2003). Those observations indicate

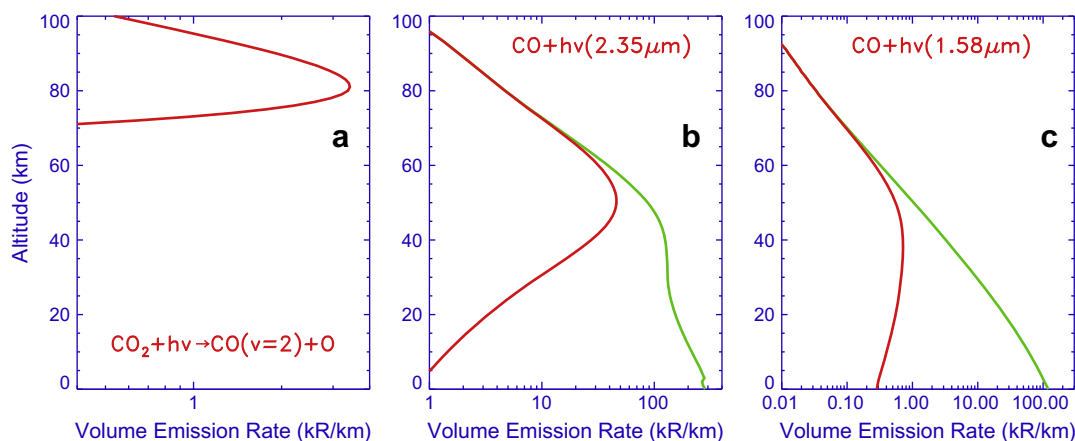
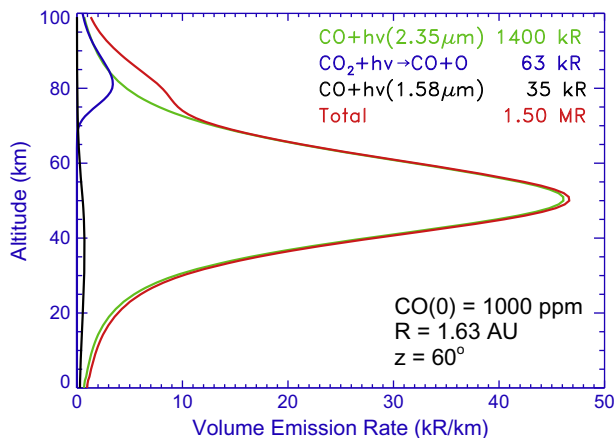
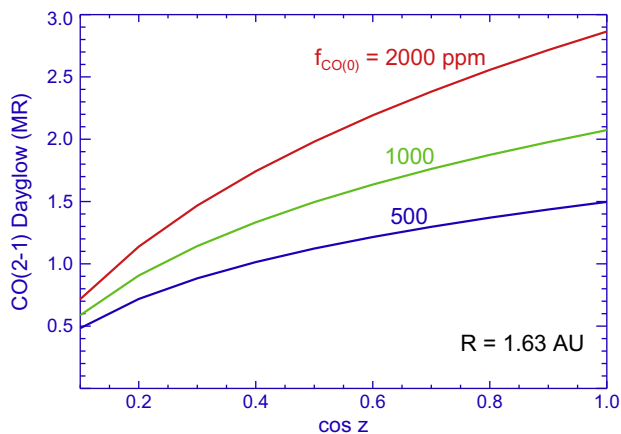


Fig. 10. Three processes of the CO (2-1) dayglow excitation. Green curves in b and c are uncorrected for quenching by  $\text{CO}_2$ . (For interpretation of the references to color in this figure legend, the reader is referred to the web version of this article.)



**Fig. 11.** Vertical profile of the CO (2-1) dayglow for the mean conditions. Three excitation processes and their sum are shown.



**Fig. 12.** Vertical intensities of the CO (2-1) dayglow versus cosine of the solar zenith angle for three adopted CO mixing ratios in the lower atmosphere.

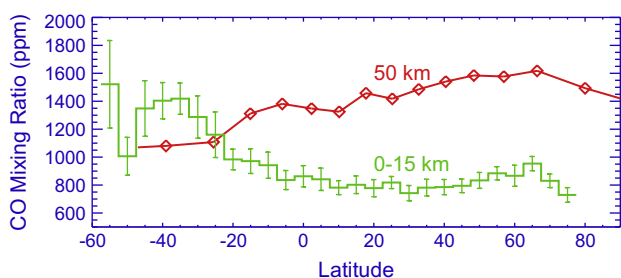


**Fig. 13.** Retrieved CO mixing ratios at 50 km are compared with those observed in the lower atmosphere at the same season in March 1999 (from Krasnopolsky, 2007).

an increase in CO to the southern subpolar latitudes that was explained by enrichment of incondensable gases in the southern winter because of condensation of CO<sub>2</sub>, and later GRS observations of argon from the Mars Odyssey orbiter (Sprague et al., 2004, 2012) confirmed this phenomenon and its interpretation. Evidently the retrieved behavior of CO at 50 km is opposite to that in the lower atmosphere. This is a diagnostics of complicated dynamical processes in the martian atmosphere that require further study in both observation and theory. The CO (2-1) dayglow is a tool for remote sensing of temperature and CO at 50 km on Mars using ground-based and spacecraft instruments. The observed CO and temperatures may be used to test photochemical GCMs for Mars.

## 7. Conclusions

We observed the CO (2-1) and (1-0) dayglow at 4.7 μm on Mars at the peak of northern summer ( $L_S = 110^\circ$ ) using the CSHELL spectrograph at NASA IRTF. Six (2-1) and two (1-0) emission lines are present in the observed spectra. These lines are contaminated by the solar CO lines and some martian and telluric lines. Intensities of the dayglow lines and reflectivities of Mars at 4.7 μm were obtained by fitting of the observed spectra by synthetic spectra.

Mean reflectivity at 109°W from 50°S to 50°N is 0.15, similar to that observed by Mariner 6 and 7 in four regions on Mars. The CO (1-0) dayglow is excited by absorption of sunlight at 4.7 μm; the emission is optically thick with a non-LTE line distribution and peaks near 87 km. The (1-0) line intensities are converted to the (1-0) band intensity using the line distribution from Billebaud et al. (1991). The measured mean intensity of the CO (1-0) dayglow is 1.7 MR with a weak limb darkening to 1.3 MR. This dayglow is poorly accessible for diagnostics of the martian atmosphere.

The CO (2-1) dayglow is excited by absorption of the sunlight by the CO (2-0) band at 2.35 μm with minor contributions from photolysis of CO<sub>2</sub> and the CO (3-0) band at 1.57 μm. The dayglow excitation by photolysis of CO<sub>2</sub> is reduced by an order of magnitude, taking into account other degrees of freedom in the CO–O system. The dayglow is quenched by CO<sub>2</sub> and peaks at 50 km. Intensities of the observed six (2-1) lines result in rotational temperatures that should be equal to ambient temperatures at 50 km. These temperatures are retrieved from 50°S to 90°N and vary in the range of 140–170 K with a mean value of 153 K.

The observed intensities of the CO (2-1) dayglow are corrected for airmass and the surface reflection and give vertical intensities that are equal to 2.1 MR at 20–50°N decreasing to 1.5 MR at 90°N and 1 MR at 45°S. The dayglow intensities depend on CO mixing ratio at 50 km and solar zenith angle. Retrieved CO mixing ratios at 50 km gradually increase from 1100 ppm at 40°S to 1600 ppm at 70°N.

This behavior is very different from that observed in the lowest scale height at the same season with increase to southern polar regions because of condensation of CO<sub>2</sub> near the south pole (Krasnopolsky, 2003). The difference reflects complicated dynamic processes in the atmosphere. This is the first observation of CO in the middle atmosphere of Mars, and the observed behavior of CO should be further studied in both observation and theory. The CO (2-1) dayglow at 4.7 μm is a tool for remote sensing of temperature and CO abundance and their variations at 50 km on Mars.

## Acknowledgments

This work is supported by NASA Planetary Astronomy Program (Grant NNX12AG28G to V.A. Krasnopolsky) and by a grant of the Russian Government to Moscow Institute of Physics and Technology (PhysTech) and V.A. Krasnopolsky.

## References

- Billebaud, F., Crovisier, J., Lellouch, E., Encrenaz, T., Maillard, J.P., 1991. High-resolution infrared spectrum of CO on Mars: Evidence for emission lines. *Planet. Space Sci.* 39, 213–218.
- Erard, S., Calvin, W., 1997. New composite spectra of Mars, 0.4–5.7 μm. *Icarus* 130, 449–460.
- Farmer, C.B., Norton, R.H., 1989. A High-Resolution Atlas of the Infrared Spectrum of the Sun and the Earth Atmosphere from Space. I. The Sun, vol. 1. NASA Ref. Publication 1224.
- Forget, F. et al., 1999. Improved general circulation models of the martian atmosphere from the surface to above 80 km. *J. Geophys. Res.* 104, 24155–24175.
- Formisano, V., Maturilli, A., Giuranna, M., D'Aversa, E., Lopez-Valverde, M.A., 2006. Observations of non-LTE emission at 4–5 microns with the Planetary Fourier Spectrometer aboard the Mars Express mission. *Icarus* 182, 51–67.

- Gilli, G. et al., 2011. Non-LTE CO limb emission at 4.7  $\mu\text{m}$  in the upper atmospheres of Venus, Mars, and Earth: Observations and modeling. *Planet. Space Sci.* 59, 1010–1018.
- Greene, T.P., Tokunaga, A.T., Toomey, D.W., Carr, J.S., 1993. CSHELL: A high spectral resolution echelle spectrograph for the IRTF. *Proc. SPIE* 1946, 313–323.
- Hase, F., Wallace, L., McLeod, S.D., Harrison, J.J., Bernath, P.F., 2010. The ACE-FTS atlas of the infrared solar spectrum. *J. Quant. Spectrosc. Radiat. Trans.* 111, 521–528.
- Krasnopolsky, V.A., 2003. Mapping of Mars O<sub>2</sub> 1.27  $\mu\text{m}$  dayglow at four seasonal points. *Icarus* 165, 315–325.
- Krasnopolsky, V.A., 2007. Long-term spectroscopic observations of Mars using IRTF/CSHELL: Mapping of O<sub>2</sub> dayglow CO, and search for CH<sub>4</sub>. *Icarus* 190, 93–102.
- Krasnopolsky, V.A., 2010. Solar activity variations of thermospheric temperatures on Mars and a problem of CO in the lower atmosphere. *Icarus* 207, 638–647.
- Krasnopolsky, V.A., Belyaev, D.A., Gordon, I.E., Li, G., Rothman, L.S., 2013. Observations of D/H ratios in H<sub>2</sub>O, HCl, and HF on Venus and new DCl and DF line strengths. *Icarus* 224, 57–65.
- McCleese, D.J. et al., 2010. Structure and dynamics of the martian lower and middle atmosphere as observed by the Mars Climate Sounder: Seasonal variations in zonal mean temperature, dust, and water ice aerosols. *J. Geophys. Res.* 115, E12016. <http://dx.doi.org/10.1029/2010JE003677>.
- Nier, A.O., McElroy, M.B., 1977. Composition and structure of Mars' upper atmosphere: Results from the neutral mass spectrometer on Viking 1 and 2. *J. Geophys. Res.* 82, 4341–4358.
- Pierce, A.K., Allen, R.G., 1977. The solar spectrum between 0.3 and 10  $\mu\text{m}$ . In: White, O.R. (Ed.), *The Solar Output and Its Variation*. Colo. Assoc. Univ. Press, Boulder, pp. 169–192.
- Rothman, L.S. et al., 2013. The HITRAN 2012 molecular spectroscopic database. *J. Quant. Spec. Rad. Tran.* 130, 4–50.
- Slanger, T.G., Black, G., 1971. The CO<sub>2</sub> photolysis problem. *J. Chem. Phys.* 54, 1889–1898.
- Smith, M.D., 2004. Interannual variability in TES atmospheric observations of Mars during 1999–2003. *Icarus* 167, 148–165.
- Sprague, A.L. et al., 2004. Mars' south polar Ar enhancement: A tracer for south polar seasonal meridional mixing. *Science* 306, 1364–1367.
- Sprague, A.L. et al., 2012. Interannual similarity and variation in seasonal circulation of Mars' atmospheric Ar as seen by the Gamma Ray Spectrometer on Mars Odyssey. *J. Geophys. Res.* 117, E04005.
- Starr, D.F., Hancock, J.K., 1975. Vibrational energy transfer in CO<sub>2</sub>–CO mixtures from 163 to 406 K. *J. Chem. Phys.* 63, 4730–4734.
- Sung, K., Varanasi, P., 2005. CO<sub>2</sub>-broadened half-widths and CO<sub>2</sub>-induced line shifts of <sup>12</sup>C<sup>16</sup>O relevant to the atmospheric spectra of Venus and Mars. *J. Quant. Spectrosc. Radiat. Trans.* 91, 319–332.
- Yoshino, K., Esmond, J.R., Sun, Y., Parkinson, W.H., Ito, K., Matsui, T., 1996. Absorption cross section measurements of carbon dioxide in the wavelength region 118.7–175.5 nm and the temperature dependence. *J. Quant. Spectrosc. Radiat. Trans.* 55, 53–60.